THE JOURNAL OF PHYSICAL CHEMISTRY C

Article

pubs.acs.org/JPCC

Structural and Electronic Properties of $AuSi_n^-$ (n = 4−12) Clusters: Photoelectron Spectroscopy and Ab Initio Calculations

Sheng-Jie Lu,[†,‡] Xi-Ling Xu,[†,‡] Gang Feng,[†,‡] Hong-Guang Xu,[*,†,‡] and Wei-Jun Zheng[*,†,‡]

[†]Beijing National Laboratory for Molecular Sciences (BNLMS), State Key Laboratory of Molecular Reaction Dynamics, Institute of Chemistry, Chinese Academy of Sciences, Beijing 100190, China

[‡]University of Chinese Academy of Sciences, Beijing 100049, China

Supporting Information

ABSTRACT: $AuSi_n^-$ (n = 4−12) clusters were produced with a laser vaporization source and investigated by photoelectron spectroscopy. The swarm-intelligence-based CALYPSO structure search method and ab initio calculations were employed to determine their ground-state structures. The results revealed that the most stable isomers of $AuSi_n^-$ (n = 4−12) cluster anions are all exohedral structures, in which the Au atom caps the vertex, edge, or surface of the bare Si_n clusters. The endohedral and exohedral structures of neutral $AuSi_{11}$ are nearly degenerate in energy. The most stable structure of neutral $AuSi_{12}$ is endohedral. The growth mechanism of $AuSi_n^-$ cluster anions is compared with those of $AuGe_n^-$, $AgSi_n^-$, and $CuSi_n^-$ clusters. It implies that the bond strengths of Au−Si and Au−Ge play important roles in the formation of cage structures for $AuSi_{12}^-$ and $AuGe_{12}^-$, while the different atomic radii of coinage metals, different bond strengths, and the strong relativistic effect in Au atom are responsible for the different growth mechanisms of Si clusters doped with different coinage metals.

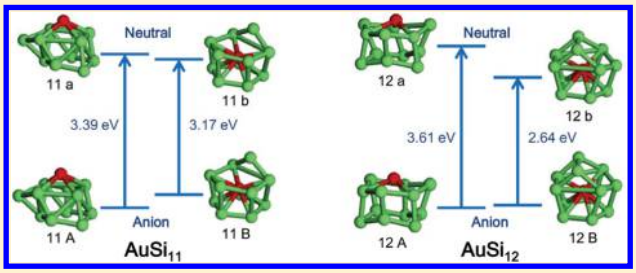

1. INTRODUCTION

Silicon is a very important element with wide applications in the catalyst industry, microelectronics, and spintronics.[1,2] Studies showed that a transition-metal (TM) atom doped into silicon clusters can stabilize fullerene-like cage structures and may lead to unusual properties, such as size selectivity, different charge transfer, large HOMO−LUMO gap, and tunable magnetic properties.[3−6] The TM-doped silicon clusters with special structures may be used as potential building blocks to fabricate the novel nanostructured materials with tunable optical, electronic, and magnetic properties. Thus, the structures and properties of TM-doped silicon clusters have been investigated extensively by experiments and theoretical calculations in the past decades.[7−33]

Gold is widely used in catalysis, medicine, electron transport, nonlinear optics, luminescence, and electronics.[34−40] The chemical properties of gold are very different from those of the other metals due to its large electronegativity, high electron affinity, and strong relativistic effects.[41,42] Hence, the structural and electronic properties of Au-doped silicon clusters may be different from the silicon clusters doped with the other transition metals. Previous theoretical studies suggested that Schottky junctions can be formed in nanoscale Au−Si systems,[43] which are important for developing high-performance solar cells. It has also been found that the vapor−liquid−solid growth of high-quality Si nanowires strongly relies on the stability of the liquid Au seed and liquid AuSi layers.[44,45] Very recently, an investigation of the metal−semiconductor alloying reaction revealed that the formation of ultrathin AuSi eutectic liquid layers can strongly enhance the alloying reaction rate due to the strain-induced chemical potential increase.[46] Exploring the structural and electronic properties of Au-doped silicon clusters not only can provide valuable information for the production of functional materials for microelectronic devices and solar cells, but also is important for understanding the microscopic mechanisms in gold-catalyzed growth of Si nanowires and metal−semiconductor alloys.

The structures of Au-doped silicon clusters and the low-lying states of the AuSi molecule were studied by theoretical calculations previously,[47−50] and the far-infrared spectra of $AuSi_n^+$ (n = 2−11, 14, 15)[51] and the photoelectron spectra of $SiAu_4^-$, $Si_2Au_n^-$ (n = 2 and 4), and $Si_3Au_3^-$ were measured by experiments.[52−54] To obtain more detailed information about the structural and electronic properties of $AuSi_n$ clusters, here we investigated the $AuSi_n^-$ (n = 4−12) clusters with anion photoelectron spectroscopy and ab initio calculations.

2. EXPERIMENTAL AND THEORETICAL METHODS

2.1. Experimental Method. The experiments were carried out on a home-built apparatus composed of a laser vaporization supersonic cluster source, a time-of-flight mass spectrometer, and a magnetic-bottle photoelectron spectrometer, which has been described elsewhere.[55] The $AuSi_n^-$ cluster anions were produced in the laser vaporization source by laser ablation of a

Received: August 25, 2016
Revised: October 16, 2016
Published: October 18, 2016

DOI: 10.1021/acs.jpcc.6b08598
J. Phys. Chem. C 2016, 120, 25628−25637

rotating and translating isotopically enriched (^{28}Si 99.989%) Au/^{28}Si disk target (Au:^{28}Si mole ratios 2:1 and 1:8, 13 mm diameter) with the second harmonic (532 nm) light pulses from a Nd:YAG laser (Continuum Surelite II-10), while helium carrier gas with ~0.4 MPa backpressure was allowed to expand through a pulsed valve (General Valve Series 9) over the AuSi target to cool the $AuSi_n^-$ clusters. The produced cluster anions were mass-analyzed by the time-of-flight mass spectrometer. The $AuSi_n^-$ (n = 4−12) clusters were each selected by a mass gate, decelerated by a momentum decelerator, and crossed by the laser beam of another Nd:YAG laser (Continuum Surelite II-10, 266 nm) at the photodetachment region. The electrons from photodetachment were energy-analyzed by the magnetic-bottle photoelectron spectrometer. The photoelectron spectra were calibrated with the spectra of Cu^- and Au^- anions taken under similar conditions. The resolution of the magnetic-bottle photoelectron spectrometer was ~40 meV for electrons with 1 eV kinetic energy.

2.2. Theoretical Method. The geometric optimizations and frequency analyses of $AuSi_n^-$ (n = 4−12) and their neutral counterparts were conducted using density-functional theory (DFT) with Becker's three-parameter and Lee−Yang−Parr's gradient-corrected correlation hybrid functional (B3LYP),[56,57] as implemented in the Gaussian 09 program package.[58] We used Pople's all-electron 6-311+G(d) basis set for the Si atoms and the scalar relativistic effective core potential Stuttgart/Dresden(SDD) basis set[59] for the Au atom. The initial structures of $AuSi_n^-$ cluster anions for geometry optimizations were obtained from the $AuSi_n^{0/+}$, $AgSi_n^{-/0/+}$, and $CuSi_n^{-/0/+}$ clusters reported in the literature[6,25,30,31,49−51,60−62] and also by putting the Au atom to different adsorption or substitution sites of the low-lying isomers of pure silicon clusters. Additionally, we have also used the swarm-intelligence-based CALYPSO structure search method[63] to construct initial structures. This method is based on the generalization of particle swarm optimization (PSO). A large number of low-energy initial structures are randomly generated with the constraint of symmetries. The Metropolis criterion and bond characterization matrix (BCM) are incorporated into the method to further enhance the structural evolution and measure of the structural similarity toward low-energy regions of potential energy surfaces. All the geometric optimizations were conducted without any symmetry constraint. As a Au atom has only one unpaired electron ($5d^{10}6s^1$), the spin singlet states of $AuSi_n^-$ cluster anions and the doublet states of their neutral counterparts were taken into account. Harmonic vibrational frequencies were analyzed to make sure that each structure corresponds to a real local minimum on the potential energy surfaces. The generalized gradient approximation in the Perdew−Burke−Ernzerhof (PBE) functional[64] was also tested for comparison. We found that the results from the B3LYP functional are in better agreement with the experiments than those from the PBE functional, so we only present the results from the B3LYP functional in this paper. To obtain the relative energies for the low-lying isomers of $AuSi_n^-$ more precisely, the single-point energies of $AuSi_n^-$ were calculated with the coupled-cluster methods including single, double, and perturbative triple excitation [CCSD(T)][65] combining the aug-cc-pVTZ-PP basis set[66] (for the Au atom) and cc-pVDZ basis set[67] (for the Si atoms). The relative energies were corrected by the zero-point vibrational energies obtained with the B3LYP functional. The natural population analysis (NPA) of $AuSi_n^-$ (n = 4−12) cluster anions was performed with the Natural Bond Orbital (NBO) version 3.1 program[68−74] in the Gaussian 09 program package.

3. EXPERIMENTAL RESULTS

The photoelectron spectra of $AuSi_n^-$ (n = 4−12) clusters recorded with 266 nm photons are presented in Figure 1. The

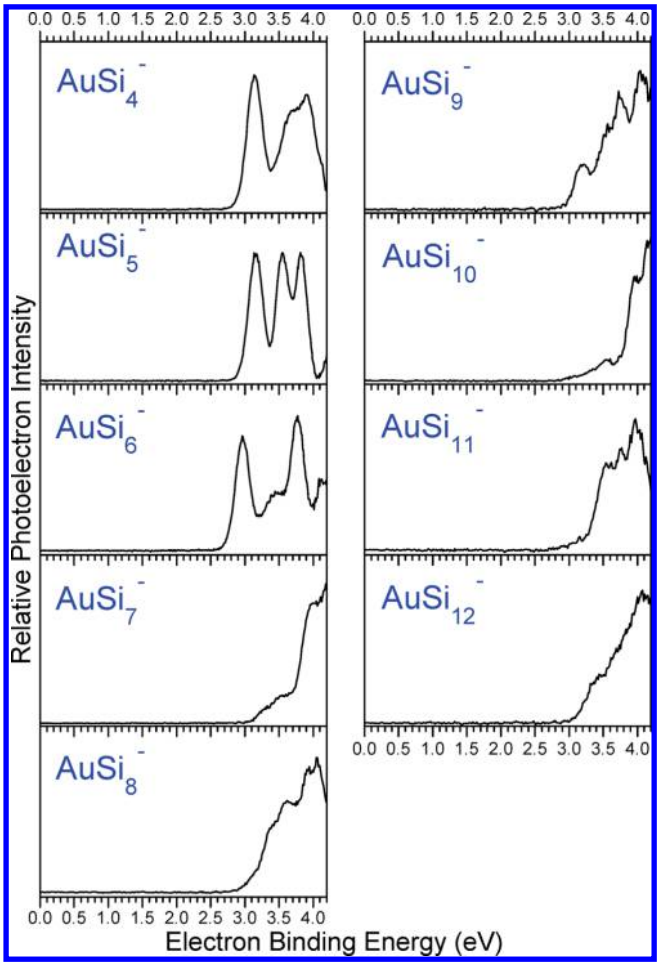

Figure 1. Photoelectron spectra of $AuSi_n^-$ (n = 4−12) clusters recorded with 266 nm photons.

experimental vertical detachment energies (VDEs) and adiabatic detachment energies (ADEs) of $AuSi_n^-$ (n = 4−12) estimated from the photoelectron spectra are shown in Table 1. As shown in Figure 1, the spectrum of $AuSi_4^-$ reveals a relatively sharp peak at 3.14 eV, and two barely resolved peaks at 3.71 and 3.91 eV. The spectrum of $AuSi_5^-$ has a prominent peak at 3.16 eV and two closely spaced peaks at 3.55 and 3.82 eV. In additional, the onset of the fourth peak is observed above 4.2 eV. The spectrum of $AuSi_6^-$ displays two high-intensity peaks at 2.96 and 3.77 eV, and two low-intensity peaks at 3.47 and 4.13 eV. The spectrum of $AuSi_7^-$ shows a broad, weak peak at 3.55 eV and a broad, strong peak at 3.99 eV. In the spectrum of $AuSi_8^-$, there is a shoulder peak at 3.39 eV, followed by three barely resolved peaks at 3.60, 3.91, and 4.05 eV, respectively. The spectrum of $AuSi_9^-$ presents four congested peaks at 3.17, 3.57, 3.73, and 4.04 eV, respectively. The spectrum of $AuSi_{10}^-$ reveals a broad, low electron binding energy (EBE) feature in the range of 3.00−3.65 eV, followed by two high-intensity peaks at 3.95 and 4.18 eV in the high-EBE region. For the spectrum of $AuSi_{11}^-$, there are three not well-separated peaks at

DOI: 10.1021/acs.jpcc.6b08598
J. Phys. Chem. C 2016, 120, 25628−25637

Table 1. Relative Energies, Theoretical VDEs and ADEs of the Low-Lying Isomers of $AuSi_n^-$ (n = 4−12) Clusters, as well as the Experimental VDEs and ADEs Estimated from Their Photoelectron Spectra[a]

isomer		ΔE[b] (eV)	VDE (eV) theor[c]	VDE (eV) expt[d]	ADE (eV) theor[c]	ADE (eV) expt[d]	isomer		ΔE[b] (eV)	VDE (eV) theor[c]	VDE (eV) expt[d]	ADE (eV) theor[c]	ADE (eV) expt[d]
$AuSi_4^-$	**4A**	0.00	3.06	3.14	2.74	2.86	$AuSi_9^-$	**9A**	0.00	3.24	3.17	2.93	2.94
	4B	0.30	3.12		2.75			**9B**	0.10	3.05		2.86	
	4C	0.35	3.06		2.76			**9C**	0.18	3.28		3.02	
	4D	0.69	2.38		2.26			**9D**	0.19	3.60		3.33	
$AuSi_5^-$	**5A**	0.00	3.06	3.16	2.80	2.88	$AuSi_{10}^-$	**10A**	0.00	3.89	3.95	3.39	3.60
	5B	0.22	3.41		2.80			**10B**	0.15	3.41	3.52	3.18	3.02
	5C	0.31	3.34		3.09			10C	0.37	3.54		3.21	
	5D	0.61	3.14		2.82			10D	0.38	3.66		3.12	
$AuSi_6^-$	**6A**	0.00	3.35	3.47	2.91	2.90	$AuSi_{11}^-$	**11A**	0.00	3.39	3.54	3.20	3.21
	6B	0.09	2.99	2.96	2.93	2.72		11B	0.11	3.17		2.99	
	6C	0.36	2.76		2.54			11C	0.26	3.36		3.16	
	6D	0.44	2.77		2.66			11D	0.34	3.22		2.83	
$AuSi_7^-$	**7A**	0.00	3.52	3.55	3.21	3.05	$AuSi_{12}^-$	**12A**	0.00	3.61	3.46	3.30	3.09
	7B	0.46	3.05		2.53			12B	0.01	2.64		2.57	
	7C	0.50	3.26		3.09			**12C**	0.17	3.33		3.17	
	7D	0.74	3.38		3.20			12D	0.43	3.28		2.12	
$AuSi_8^-$	**8A**	0.00	3.22	3.39	3.11	3.04							
	8B	0.04	3.15		2.91								
	8C	0.05	3.48		3.21								
	8D	0.19	3.58		3.21								

[a]The isomers labeled in bold are the most probable ones in the experiments. [b]The ΔEs values are calculated at the CCSD(T)/aug-cc-pVTZ-PP/Au/cc-pVDZ/Si level of theory. [c]The ADEs and VDEs are calculated at the B3LYP/SDD/Au/6-311+G(d)/Si level of theory. [d]The uncertainties of the experimental VDEs and ADEs are ±0.08 eV.

3.54, 3.77, and 3.98 eV, respectively. In the spectrum of $AuSi_{12}^-$, we can roughly distinguish a low-intensity, broad peak at ∼3.46 eV and a high-intensity, broad peak at ∼4.06 eV.

It is worth mentioning that $Au^{28}Si_n^-$ is heavier than $^{28}Si_{n+7}^-$ ($n \geq 0$) by only 1 amu and it is also lighter than $Au_2{}^{28}Si_{n-7}^-$ ($n \geq 7$) by only 1 amu. Thus, the mass peaks of $^{28}Si_{n+7}^-$ and $Au^{28}Si_n^-$ are separated by only one amu in the order of $^{28}Si_{n+7}^-$ < $Au^{28}Si_n^-$, and for $n \geq 7$, the mass peaks of $Au^{28}Si_n^-$ and $Au_2{}^{28}Si_{n-7}^-$ are separated by only one amu in the order of $Au^{28}Si_n^-$ < $Au_2{}^{28}Si_{n-7}^-$. Our TOF mass spectrometer was able to resolve the mass peaks of $Au^{28}Si_n^-$ with n up to 12. To make sure that the photoelectron spectra of $Au^{28}Si_n^-$ are not contaminated by the spectra of $^{28}Si_{n+7}^-$, we have also compared the spectra of $Au^{28}Si_n^-$ clusters with the photoelectron spectra of Si_{n+7}^- clusters in the literature.[75] Additionally, we have measured the photoelectron spectra of $Au_2{}^{28}Si_n^-$ (n = 0−5) which were produced by ablating an isotopically enriched (^{28}Si 99.989%) Au/^{28}Si disk target of much higher Au:^{28}Si mole ratio and compared them with those of $Au^{28}Si_{7-12}^-$ to ensure that the spectra of $Au^{28}Si_{7-12}^-$ are not contaminated by the signals from $Au_2{}^{28}Si_{0-5}^-$.

4. THEORETICAL RESULTS

The structures of the low-lying isomers of $AuSi_n^-$ (n = 4−12) clusters obtained from the ab initio calculations are presented in Figure 2. The relative energies (ΔE) and theoretical VDEs and ADEs of these low-lying isomers are summarized in Table 1, along with the experimental VDEs and ADEs for comparison.

We also performed simulations on the photoelectron spectra of the low-lying isomers of $AuSi_n^-$ (n = 4−12) based on the generalized Koopmans' theorem (GKT).[76,77] In the simulated spectra, each peak corresponds to the removal of an electron from an individual molecular orbital of the cluster anion. We first set the peak from the highest occupied molecular orbital (HOMO) at the position of the calculated VDE of each isomer, and the other peaks related to the deeper orbitals are shifted to the higher EBE side in terms of their relative energies to the HOMO. For convenience, the simulated photoelectron spectra are called density of states (DOS) spectra. The comparison of the DOS spectra and experimental spectra of $AuSi_n^-$ (n = 4−12) are displayed in Figure 3.

4.1. $AuSi_4^-$. The first isomer of $AuSi_4^-$ (4A) has the Au atom interacting with one Si atom of the Si_4 rhombus while its second isomer (4B) has the Au atom interacting with one Si atom of the Si_4 tetrahedron. Isomer 4C has a pyramid structure with the Au atom interacting with three Si atoms. In isomer 4D, the Au atom interacts with three Si atoms of the Si_4 kite-shaped structure. The calculated VDE of isomer 4A is 3.06 eV, which is in agreement with the experimental VDE (3.14 eV), and its DOS spectrum fits well with the peak positions and patterns of the experimental spectrum. Thus, we suggest that isomer 4A is the most probable one observed in the experiments, and the existence of isomers 4B, 4C and 4D can be ruled out because they are higher in energy than isomer 4A by at least 0.30 eV.

4.2. $AuSi_5^-$. Our calculations showed that isomers 5A, 5C, and 5D all possess a Si_5 trigonal bipyramid subunit with the Au atom interacting with the surface or different Si atoms of the Si_5 subunit. Isomer 5B can be viewed as deriving from isomer 4A by an additional Si atom face-capping the Si_4 rhombus. Isomers 5B, 5C, and 5D are higher in energy than isomer 5A by 0.22, 0.31, and 0.61 eV, respectively. The calculated VDE of isomer 5A is 3.06 eV, which is in good agreement with the experimental value (3.16 eV), and its simulated DOS spectrum fits the peak positions and patterns of the experimental spectrum very well. As a result, we suggest isomer 5A to be the most probable one detected in the experiments.

DOI: 10.1021/acs.jpcc.6b08598
J. Phys. Chem. C 2016, 120, 25628−25637

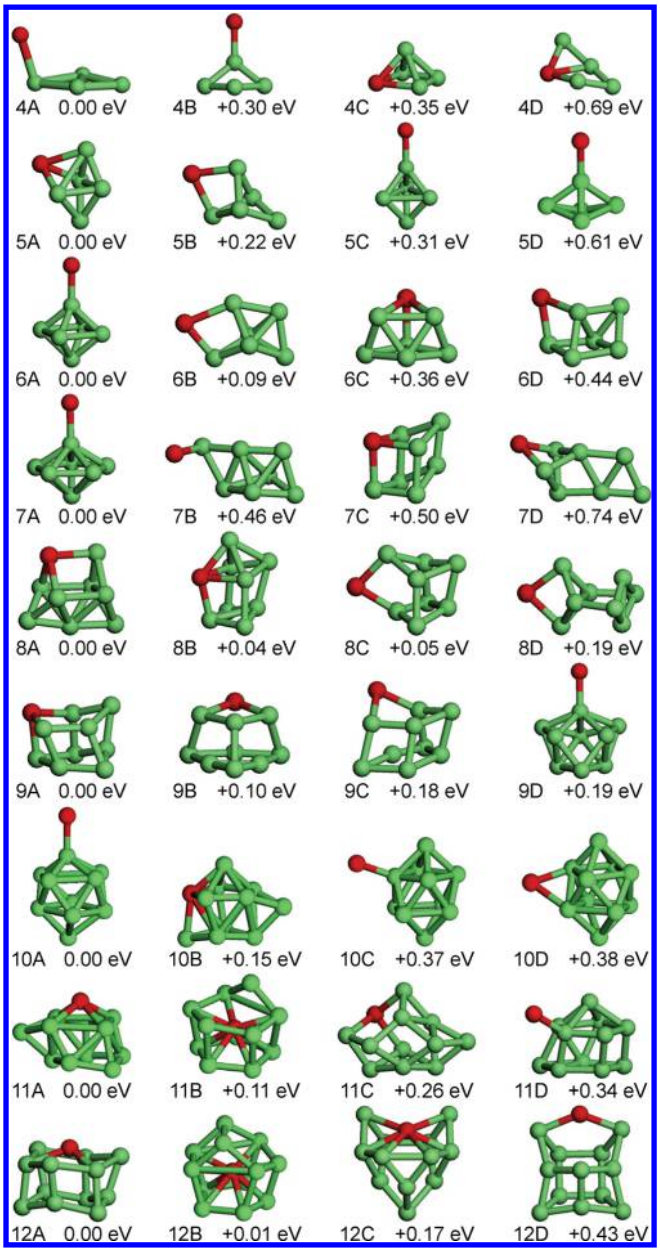

Figure 2. Typical low-lying isomers of $AuSi_n^-$ (n = 4−12) clusters. The ΔE values are calculated at the CCSD(T)/aug-cc-pVTZ-PP/Au/cc-pVDZ/Si level of theory. The green and red balls stand for the Si atoms and Au atoms, respectively.

4.3. $AuSi_6^-$. The most stable isomer of $AuSi_6^-$ (6A) is a C_{4v} symmetric structure with the Au atom interacting with one Si atom of the Si_6 tetragonal bipyramid. Isomer 6B can be considered as deriving from isomer 5B by an additional Si atom face-capping the Si_4 rhombus. For isomer 6C, the six Si atoms form a face-capping trigonal bipyramid structure, and then the Au atom interacts with the Si_6 motif by capping one of the faces. Isomer 6D can be viewed as the Au atom and an additional Si atom face-capping the Si_5 trigonal bipyramid. The calculated VDE of isomer 6A (3.35 eV) is in good agreement with the experimental peak at 3.47 eV, and that of isomer 6B (2.99 eV) is consistent with the experimental peak at 2.96 eV. The DOS spectrum of isomer 6A can match the experimental peaks at higher EBE regions and that of isomer 6B is in good agreement with the experimental peaks centered at 2.96 and 4.13 eV. The combination of the DOS spectra of isomers 6A and 6B can reproduce the peak positions and patterns of the experimental spectrum. Isomers 6C and 6D are unlikely to present in our experiments because they are higher in energy than isomer 6A by at least 0.36 eV. Therefore, we suggest that isomers 6A and 6B are the most probable species observed in our experiments. We would like to point out that the coexistence of two isomers in the experiments has also been found for $CrSi_6^-$, $CuSi_6^-$, and $AgSi_6^-$ clusters.[30,31,78]

4.4. $AuSi_7^-$. With respect to $AuSi_7^-$, isomer 7A is a C_{5v} symmetric pentagonal bipyramid with the Au atom interacting with one Si atom of the Si_7 motif. Isomer 7B can be viewed as the Au atom interacting with one Si atom of the Si_7 bicapped trigonal bipyramid. Isomer 7C can be constructed by the Au atom and an additional Si atom face-capping the Si_6 trigonal prism. Isomer 7D can be obtained by the Au atom and an additional Si atom capping the Si_6 quasiplanar structure. The calculated VDE of isomer 7A (3.52 eV) agrees well with the experimental value (3.55 eV), and the peak positions and patterns of its DOS spectrum match the experimental spectrum very well. Isomers 7B, 7C, and 7D are not expected to be populated in the experiments because they are significantly higher in energy than isomer 7A by at least 0.46 eV. Thus, we suggest that isomer 7A is the most probable one contributing to the photoelectron spectrum of $AuSi_7^-$.

4.5. $AuSi_8^-$. The lowest-lying isomer of $AuSi_8^-$ (8A) can be viewed as the Au atom face-capping the Si_8 bicapped tetragonal bipyramid. Isomer 8B can be constructed by an additional Si atom capping the top face of isomer 7C. Isomer 8C can be regarded as the Au atom capping the Si−Si bond of the Si_8 tetragonal prism. Isomer 8D can be considered as the Au atom capping the Si−Si bond of a distorted Si_8 bicapped tetragonal bipyramid. The calculated VDE of isomer 8A (3.22 eV) is in reasonable agreement with the experimental value (3.39 eV), and its DOS spectrum fits the peak positions and patterns of the experimental spectrum. The calculated VDEs of isomers 8B and 8C (3.15 and 3.48 eV) are in reasonable agreement with the experimental value and they are higher in energy than isomer 8A by only 0.04 and 0.05 eV, respectively. Isomer 8D is higher in energy than 8A by 0.19 eV, and its calculated VDE (3.58 eV) is also in reasonable agreement with the experimental value. Thus, we suggest that isomer 8A is the most probable one detected in the experiments and that isomers 8B, 8C, and 8D may also contribute to the photoelectron spectrum of $AuSi_8^-$. The coexistence of multiple isomers can explain why the spectral features of $AuSi_8^-$ are very broad.

4.6. $AuSi_9^-$. As shown in Figure 2, isomer 9A of $AuSi_9^-$ can be regarded as the Au atom replacing one Si atom of a distorted Si_{10} pentagonal prism. Isomer 9B can be viewed as the Au atom substituting for one Si atom of the Si_4 rhombus interconnected with the Si_6 six-membered ring. Isomer 9C can be viewed as deriving from isomer 9A by stretching the Au−Si bond length. In isomer 9D, the Au atom interacts with one Si atom of the Si_9 tricapped trigonal prism (TTP) structure, which is the main subunit of Si_n clusters in the range of n = 10−20.[79] Isomers 9B, 9C, and 9D are higher in energy than isomer 9A by 0.10, 0.18, and 0.19 eV, respectively. The calculated VDE of isomer 9A (3.24 eV) is in excellent agreement with the experimental value (3.17 eV) and its simulated DOS spectrum is in reasonable agreement with the experimental spectrum. Thus, we suggest that isomer 9A is the most probable one detected in our experiments, and isomers 9B, 9C, and 9D may also contribute to the experimental spectrum of $AuSi_9^-$.

DOI: 10.1021/acs.jpcc.6b08598
J. Phys. Chem. C 2016, 120, 25628−25637

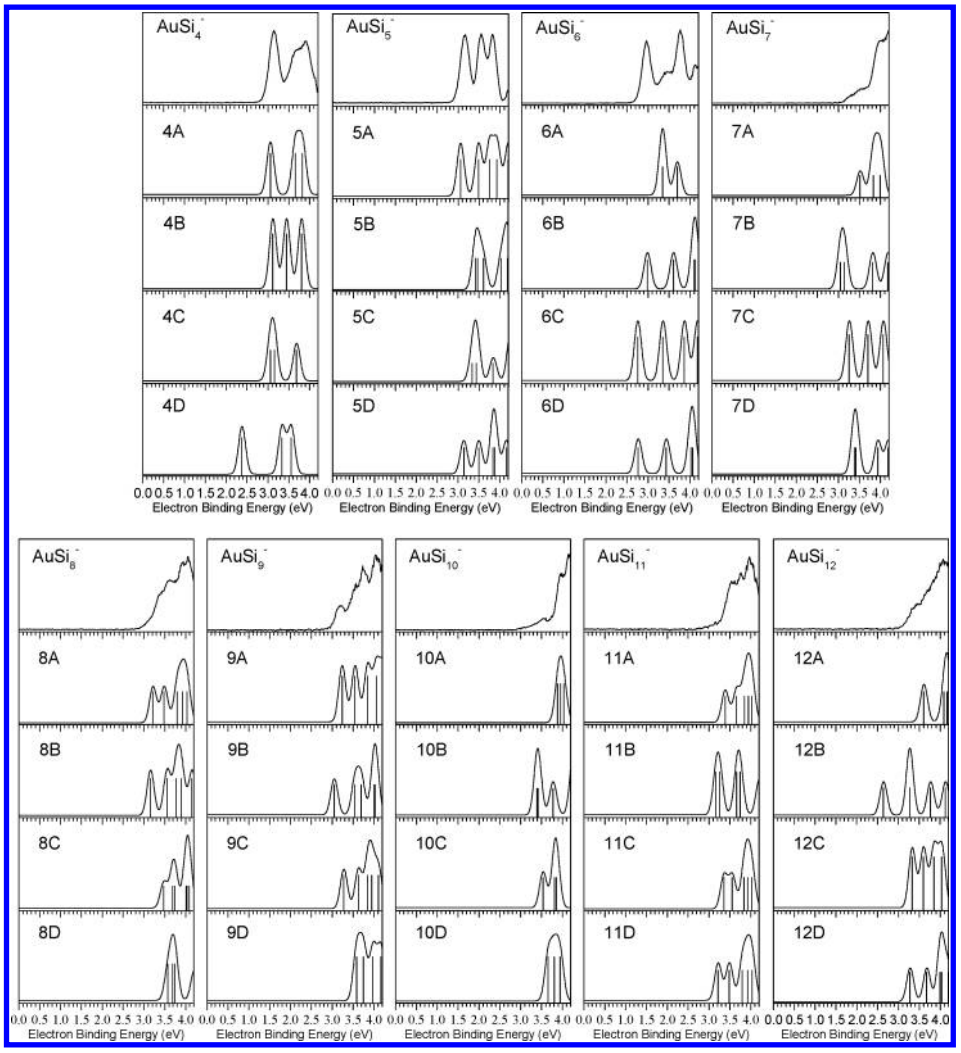

Figure 3. Comparison between the experimental photoelectron spectra and the simulated DOS spectra of the low-lying isomers of $AuSi_n^-$ (n = 4–12) clusters is shown. The simulated spectra were obtained by fitting the distribution of the transition lines with the unit area Gaussian functions of 0.20 eV full widths at half-maximum.

4.7. $AuSi_{10}^-$. In isomers 10A, 10C, and 10D of $AuSi_{10}^-$, the 10 Si atoms form a bicapped tetragonal antiprism, and the Au atom interacts with the Si_{10} motif by capping its vertex and edge. Isomer 10B has the Au atom and two additional Si atoms face-capping the Si_8 tetragonal antiprism, and it is higher in energy than isomer 10A by 0.15 eV. The calculated VDE of 10A (3.89 eV) is in good agreement with the spectral feature at 3.95 eV in the experimental spectrum of $AuSi_{10}^-$, while the theoretical VDE (3.41 eV) of isomer 10B is consistent with the broad, low EBE feature in the range of 3.00–3.65 eV. The combination of the DOS spectra of isomers 10A and 10B can reproduce the peak positions and patterns of the experimental spectrum. Thus, we suggest that isomer 10A is the major one contributing to the experimental spectrum and 10B is the minor one. The existence of isomers 10C and 10D can be ruled out because they are higher in energy than isomer 10A by at least 0.37 eV.

4.8. $AuSi_{11}^-$. For the $AuSi_{11}^-$ cluster, the lowest-lying isomer (11A) can be described as the Au atom face-capping the Si_{11} face-capped pentagonal antiprism. In isomer 11B, the Au atom is sandwiched into a pair of Si_5 five-membered rings with an additional Si atom capping one edge of one Si_5 ring, which is found to be the most stable structure for the neutral $AuSi_{11}$ cluster in the literature.[50] Isomer 11C is a close-packed structure with the Au atom capping the surface. Isomer 11D can be viewed as the Au atom interacting with one Si atom of the Si_{11} face-capped pentagonal prism. The calculated VDE of isomer 11A is 3.39 eV, which is in reasonable agreement with the experimental value (3.54 eV). Also, its simulated DOS spectrum resembles the experimental spectrum. Isomer 11B is higher in energy than isomer 11A by 0.11 eV, and its calculated VDE (3.17 eV) is much deviated from the experimental VDE. Isomers 11C and 11D are higher in energy than isomer 11A by 0.26 and 0.34 eV. Thus, we suggest isomer 11A to be the most probable one contributing to the photoelectron spectrum of $AuSi_{11}^-$.

4.9. $AuSi_{12}^-$. For the $AuSi_{12}^-$ cluster, the most stable isomer (12A) can be viewed as the Au atom face-capping the distorted Si_{12} hexagonal prism. In isomer 12B, the Au atom is sandwiched into a pair of Si_5 five-membered rings with two additional Si atoms capping one of the Si_5 rings. The capped Si_5 ring is slightly larger than the noncapped one. Isomer 12B is similar to the most stable structure of the neutral $AuSi_{12}$ cluster reported by Wang et al.[50] Isomer 12C can be regarded as a half-endohedral structure with the Au atom sitting in a V-shaped Si_{12} framework. Isomer 12D can be viewed as a handbag-like

DOI: 10.1021/acs.jpcc.6b08598
J. Phys. Chem. C 2016, 120, 25628–25637

structure in which the top three atoms (two Si atoms and one Au atom) are regarded as the handle and the remaining ten Si atoms constitute the body of the bag. The VDE of isomer 12A is calculated to be 3.61 eV, which agrees well with the experimental value (3.46 eV), and its simulated DOS spectrum is in reasonable agreement with the experimental spectrum, except that the peaks in the experimental spectrum overlap with each other due to low spectral resolution. Isomer 12B is higher in energy than isomer 12A by only 0.01 eV, but its VDE is calculated to be 2.64 eV, which is much lower than the experimental value. The theoretical VDE (3.33 eV) of isomer 12C is close to the experimental value and it is higher in energy than isomer 12A by 0.17 eV. Isomer 12D is unlikely to be populated in our experiments because it is higher in energy than isomer 12A by 0.43 eV. Therefore, we suggest that isomer 12A is the most probable one observed in our experiments and isomer 12C may make a minor contribution to the photoelectron spectrum of $AuSi_{12}^-$.

In this work, we have considered those endohedral structures reported in the literature in the structural searching for $AuSi_{11}^-$ and $AuSi_{12}^-$ clusters. We found that the basketlike endohedral structure (11B) is higher in energy than the exohedral structure (11A) by 0.11 eV, and its calculated VDE (3.17 eV) is much deviated from the experimental value (3.54 eV). The bicapped pentagonal prism (12B) is higher in energy than the exohedral structure (12A) by only 0.01 eV, but its calculated VDE (2.64 eV) is much lower than the experimental value (3.46 eV); thus, 12B is unlikely to be detected in our experiments. More likely, the relative energy between 12B and 12A is underestimated by the CCSD(T) methods.

5. DISCUSSION

Figure 4 shows the change of the experimental VDEs as well as the theoretical VDEs of the most stable isomers versus n, the

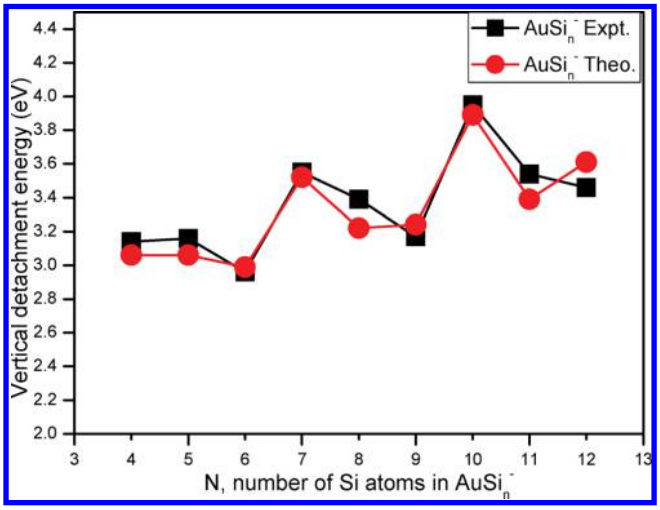

Figure 4. Experimental and theoretical VDEs of $AuSi_n^-$ (n = 4−12) clusters versus n, the number of silicon atoms.

number of silicon atoms. It can be observed in Figure 4 that the theoretical VDEs are compatible with the experimental values with average deviations of ∼0.15 eV, indicating that the theoretical methods used in this work are reliable. The comparison of theoretical calculations with experimental results showed that the most stable structures of $AuSi_n^-$ (n = 4−12) cluster anions are all exohedral structures with the Au atom capping the vertex, edge, or surface of the bare Si_n clusters.

Additionally, we have optimized the structures of neutral $AuSi_{11}$ and $AuSi_{12}$ clusters and found the most stable structures of these two clusters are endohedral, different from those of their anionic counterparts. The structures of neutral $AuSi_{11}$ and $AuSi_{12}$ as well as their anionic counterparts are displayed in Figure 5. The endohedral structure of neutral $AuSi_{11}$ (11b) is

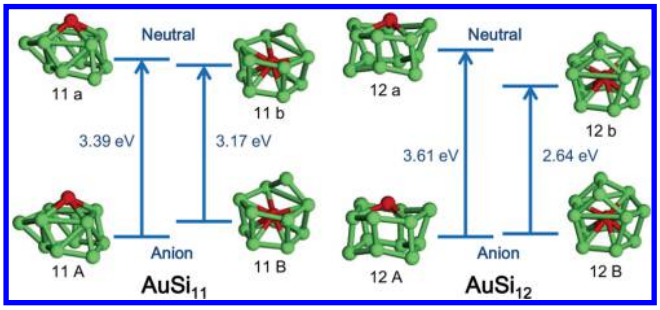

Figure 5. Transition from the anions to the neutrals for $AuSi_{11}$ and $AuSi_{12}$ clusters.

lower in energy than its exohedral structure (11a) by only 0.02 eV and the endohedral structure of neutral $AuSi_{12}$ (12b) is lower in energy than its exohedral structure (12a) by 0.72 eV, which are calculated at the CCSD(T) level of theory. Thus, the endohedral structures of neutral $AuSi_n$ clusters emerge at n = 11 and become more stable at n = 12. It seems that the removal of the excess electron from $AuSi_n^-$ anions strengthens the interactions between Au and Si. These also indicate that the excess electron has an obvious influence on the structural evolution of neutral $AuSi_n$ clusters. The endohedral structures for $AuSi_{11-12}$ clusters found by us are in agreement with the previous theoretical calculations of neutral $AuSi_n$ clusters reported by Wang et al.[50]

Here, we compare the structures of $AuSi_n^-$ with those of $AuGe_n^-$.[80] We found that the most stable structures of $AuSi_{4-5,7-8,10}^-$ are similar to those of $AuGe_{4-5,7-8,10}^-$, but those of $AuSi_{6,9,11-12}^-$ are different from those of $AuGe_{6,9,11-12}^-$. The most stable structure of $AuSi_6^-$ is a tetragonal bipyramid instead of a face-capped trigonal bipyramid as in the case of $AuGe_6^-$. The lowest-lying structure of $AuSi_9^-$ is a distorted Si_{10} pentagonal prism instead of a multirhombus prism as in the case of $AuGe_9^-$. The global minimum of $AuSi_{11}^-$ is an exohedral structure rather than an endohedral structure as in the case of $AuGe_{11}^-$. Especially, the lowest-lying isomer of $AuSi_{12}^-$ is an exohedral structure, while that of $AuGe_{12}^-$ is an I_h symmetric icosahedral endohedral structure. Why can the $AuGe_{12}^-$ cluster form a highly symmetric endohedral structure whereas the $AuSi_{12}^-$ cluster has an exohedral structure? This can be partially explained by their different bond strengths. The Au−Ge bond length (2.46 Å) is close to the Ge−Ge bond length (2.44 Å),[88] and the Au−Si bond length (2.26 Å) is also similar to the Si−Si bond length (2.24 Å).[81] The Au−Ge bond (2.84 eV) is stronger than the Ge−Ge bond (2.78 eV),[82] while the Au−Si bond (3.30 eV) is weaker than the Si−Si bond (3.37 eV).[83,84] These values imply that a Ge atom prefers to form a bond with a Au atom rather than to interact with some other Ge atoms. The formation of Au−Ge bonds can enhance the stability of the $AuGe_{12}^-$ endohedral structure compared to the formation of Ge−Ge bonds, whereas the Si atoms would prefer to form fewer Au−Si bonds and more Si−Si bonds; as a

DOI: 10.1021/acs.jpcc.6b08598
J. Phys. Chem. C 2016, 120, 25628−25637

consequence, the encapsulation of a Au atom into the Si_{12} cage would be energetically unfavorable.

It would be interesting to compare the structures of $AuSi_n^-$ with those of $CuSi_n^-$ and $AgSi_n^-$.[30,31] We found that the most stable structures of MSi_{4-7}^- (M = Au, Ag, and Cu) are very similar, but those of MSi_{8-12}^- are different. In the global minimum of $AuSi_8^-$, the Au atom and two additional Si atoms cap the Si_6 tetragonal bipyramid instead of the Ag and Cu atoms edge-capping the Si_8 tetragonal prism as in the cases of $AgSi_8^-$ and $CuSi_8^-$. As for the global minima of MSi_9^-, the Au atom replaces one Si atom of a distorted Si_{10} pentagonal prism, while the Ag atom attaches to the Si_9 TTP structure and the Cu atom caps the Si_9 boat-shaped structure. In the lowest-lying isomers of MSi_{10}^-, the Au atom interacts with one Si atom of the Si_{10} bicapped tetragonal antiprism, while the Ag atom and the 10th Si atom cap the Si_9 TTP structure, and the Cu atom substitutes for one Si atom of the Si_{11} framework. In the global minimum of $AuSi_{11}^-$, the Au atom interacts with the Si_{11} framework by capping its facet, while the Ag atom interacts with one Si atom of the Si_{11} framework and the Cu atom interacts with the surface of Si_{11} framework. Especially, at n = 12, $AuSi_{12}^-$ has the Au atom capping the distorted Si_{12} hexagonal prism while $AgSi_{12}^-$ has the Ag atom attaching to one Si atom of Si_{12} hexacapped trigonal prism, whereas the Cu atom is completely encapsulated into the Si_{12} hexagonal prism. These facts suggest that the structural evolution of coinage-metal-doped silicon clusters is different, even though they are in the same group. We would like to point out that in MSi_{12}^-, the Au atom interacts with 3 Si atoms and the Ag atom interacts with only 1 Si atom, while the Cu atom interacts with 12 Si atoms because it is completely encapsulated. Considering the coordination numbers, the order is Cu > Au > Ag, which is different from the order of these elements in the periodic table. This may be associated with the strong relativistic effect in Au atom, which is also found to be responsible for the anomalous ordering of the VDEs of $Cu(BO_2)_2$ (5.28 eV) < $Au(BO_2)_2$ (5.90 eV) < $Ag(BO_2)_2$ (6.28 eV).[85−88] The atomic radii of coinage metals are in the order of r_{Au} (1.74 Å) > r_{Ag} (1.65 Å) > r_{Cu} (1.45 Å),[89] and the bond strengths and bond lengths of coinage metal silicide are in the order of Au−Si (3.30 eV) > Cu−Si (2.29 eV) > Ag−Si (1.88 eV) and Au−Si (2.26 Å) < Cu−Si (2.28 Å) < Ag−Si (2.40 Å),[81,83,90] which can partially explain why $AuSi_{12}^-$, $AgSi_{12}^-$, and $CuSi_{12}^-$ clusters adopt different structures and also suggest that coinage metals do not follow their order in the periodic table when they interact with silicon clusters.

To give insight into the charge distributions of coinage-metal-doped Si clusters, we carried out natural population analyses (NPA) on the most stable isomers of MSi_n^- (n = 4−12) clusters, as presented in Figure 6. The lowest-lying structures of $CuSi_n^-$ (n = 4−12) and $AgSi_n^-$ (n = 4−12) clusters are obtained from our previous works.[30,31] We can see from Figure 6 that the NPA charge distributions on the coinage metal are very similar at n = 4−7, except that the NPA charges on the Au atom are all negative charges, while those on the Ag and Cu atoms are almost positive charges. However, with the increasing size of the clusters, the NPA charge distributions on the coinage metals are different; especially, the NPA charges on the Cu atom decrease significantly at n = 9 and 12. These can be explained by two reasons. First, the similar charge distributions on the coinage metals at n = 4−7 is due to the similar structures of MSi_{4-7}^-, whereas the structures of MSi_{8-12}^- are different, resulting in different charge distributions

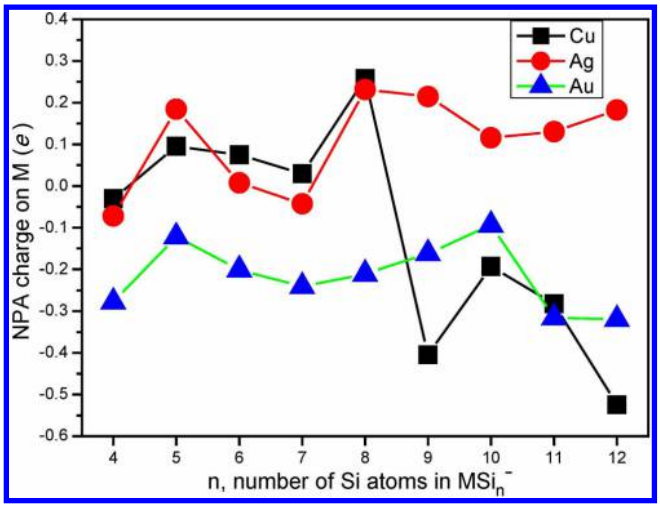

Figure 6. NPA charges on the metal atoms of the most stable isomers of MSi_n^- (M = Au, Ag, and Cu) clusters.

on the coinage metals. The unprecedented change of NPA charges on the Cu atoms at n = 9 and 12 probably is because of the formation of a $CuSi_9^-$ half-endohedral structure and a $CuSi_{12}^-$ cagelike structure. Second, the electronegativity of the Au atom (χ = 2.54) is much stronger than those of Ag atom (χ = 1.93), Cu atom (χ = 1.90), and Si atom (χ = 1.90),[91] which can explain why the NPA charges on the Au atom are all negative charges, while those on the Ag and Cu atoms are almost positive charges at small cluster sizes. Therefore, the NPA charge distributions on the coinage metals are not only associated with the structural evolution of MSi_n^- but also correlated with the electronegativities of coinage metals. The NPA charges on the Au atom are in the range of −0.09 e to −0.32 e from $AuSi_4^-$ to $AuSi_{12}^-$. The transfer of electron from the Si_n frameworks to the Au atom is more likely due to the strong electronegativity of the Au atom. The change of NPA charge versus n is not significant for $AuSi_n^-$ anions because they all have exohedral structures. The $AuSi_n^-$ anions all have closed-shell electronic structures. Thus, it is expected that they possess large HOMO−LUMO gaps. Indeed, our calculations show that the HOMO−LUMO gaps of $AuSi_n^-$ clusters range between 2.20 and 2.95 eV.

6. CONCLUSIONS

We studied the structural and electronic properties of $AuSi_n^-$ (n = 4−12) clusters with anion photoelectron spectroscopy and ab initio calculations. Our results showed that the global minima structures of $AuSi_n^-$ (n = 4−12) clusters are exohedral structures, in which the Au atom prefers to cap the vertex, edge, or surface of the Si_n frameworks. The endohedral structures of neutral $AuSi_n$ clusters emerge at n = 11 and become more stable at n = 12. The most stable structure of neutral $AuSi_{12}$ has the Au atom being sandwiched by a pair of Si_5 five-membered rings, and two additional Si atoms cap one of the Si_5 rings. The structures of $AuSi_n^-$ are compared with those of $AuGe_n^-$, $AgSi_n^-$, and $CuSi_n^-$ clusters, suggesting that the bond strengths of Au−Si and Au−Ge play important roles in the cage formation for $AuSi_{12}$ and $AuGe_{12}$ clusters, while the different atomic radii of coinage metals, different bond strengths, and the strong relativistic effect in Au atom lead to the different growth mechanisms of coinage-metal-doped silicon clusters. The structural evolution and electronic

DOI: 10.1021/acs.jpcc.6b08598
J. Phys. Chem. C 2016, 120, 25628−25637

properties of Au-doped silicon clusters revealed in this work can provide valuable information on the production of functional materials for microelectronic devices and solar cells and are also important for understanding the microscopic mechanisms in gold-catalyzed growth of Si nanowires and nanotubes.

■ ASSOCIATED CONTENT

Supporting Information

The Supporting Information is available free of charge on the ACS Publications website at DOI: 10.1021/acs.jpcc.6b08598.

The mass spectra at different sample mole ratios, the low-lying isomers of neutral $AuSi_{4-12}$ clusters, and the Cartesian coordinates of the low-lying isomers of $AuSi_{4-12}^{-/0}$ clusters (PDF)

■ AUTHOR INFORMATION

Corresponding Authors

*H.-G.X.: e-mail, xuhong@iccas.ac.cn.

*W.-J.Z.: e-mail, zhengwj@iccas.ac.cn; tel, +86 10 62635054; fax, +86 10 62563167.

Notes

The authors declare no competing financial interest.

■ ACKNOWLEDGMENTS

This work was supported by the National Natural Science Foundation of China (Grant No. 21273246 and 21103202) and the Chinese Academy of Sciences (Grant No. QYZDB-SSW-SLH024). The theoretical calculations were performed on the China Scientific Computing Grid (ScGrid) of the Supercomputing Center, Computer Network Information Center of the Chinese Academy of Sciences.

■ REFERENCES

(1) Weldon, M. K.; Queeney, K. T.; Eng, J., Jr.; Raghavachari, K.; Chabal, Y. J. The surface science of semiconductor processing: gate oxides in the ever-shrinking transistor. *Surf. Sci.* **2002**, *500*, 859−878.

(2) Zutic, I.; Fabian, J.; Sarma, S. D. Spintronics: fundamentals and applications. *Rev. Mod. Phys.* **2004**, *76*, 323−410.

(3) Singh, A. K.; Briere, T. M.; Kumar, V.; Kawazoe, Y. Magnetism in transition-metal-doped silicon nanotubes. *Phys. Rev. Lett.* **2003**, *91*, 146802.

(4) Negishi, A.; Kariya, N.; Sugawara, K. i.; Arai, I.; Hiura, H.; Kanayama, T. Size-selective formation of tungsten cluster-containing silicon cages by the reactions of with SiH_4. *Chem. Phys. Lett.* **2004**, *388*, 463−467.

(5) Robles, R.; Khanna, S. N. Magnetism in assembled and supported silicon endohedral cages: first-principles electronic structure calculations. *Phys. Rev. B: Condens. Matter Mater. Phys.* **2009**, *80*, 115414.

(6) Ma, W. Q.; Chen, F. Y. Electronic, magnetic and optical properties of Cu, Ag, Au-doped Si clusters. *J. Mol. Model.* **2013**, *19*, 4555−4560.

(7) Kumar, V.; Kawazoe, Y. Metal-encapsulated fullerenelike and cubic caged clusters of silicon. *Phys. Rev. Lett.* **2001**, *87*, 045503.

(8) Kumar, V.; Kawazoe, Y. Magic behavior of $Si_{15}M$ and $Si_{16}M$ (M = Cr, Mo, and W) clusters. *Phys. Rev. B: Condens. Matter Mater. Phys.* **2002**, *65*, 073404.

(9) Khanna, S. N.; Rao, B. K.; Jena, P. Magic numbers in metallo-inorganic clusters: chromium encapsulated in silicon cages. *Phys. Rev. Lett.* **2002**, *89*, 016803.

(10) Lu, J.; Nagase, S. Structural and electronic properties of metal-encapsulated silicon clusters in a large size range. *Phys. Rev. Lett.* **2003**, *90*, 115506.

(11) Guo, P.; Ren, Z. Y.; Wang, F.; Bian, J.; Han, J. G.; Wang, G. H. Structural and electronic properties of $TaSi_n$ (n = 1−13) clusters: a relativistic density functional investigation. *J. Chem. Phys.* **2004**, *121*, 12265−12275.

(12) Li, J. R.; Yao, C. H.; Mu, Y. W.; Wan, J. G.; Han, M. Structures and magnetic properties of Si_nNi (n = 1−17) clusters. *J. Mol. Struct.: THEOCHEM* **2009**, *916*, 139−146.

(13) Han, J. G.; Zhao, R. N.; Duan, Y. H. Geometries, stabilities, and growth patterns of the bimetal Mo_2-doped Si_n (n = 9−16) clusters: a density functional investigation. *J. Phys. Chem. A* **2007**, *111*, 2148−2155.

(14) Kong, L. Z.; Chelikowsky, J. R. Transport properties of transition-metal-encapsulated Si cages. *Phys. Rev. B: Condens. Matter Mater. Phys.* **2008**, *77*, 073401.

(15) Mpourmpakis, G.; Froudakis, G. E.; Andriotis, A. N.; Menon, M. Understanding the structure of metal encapsulated Si cages and nanotubes: role of symmetry and d-band filling. *J. Chem. Phys.* **2003**, *119*, 7498−7502.

(16) Zheng, W. J.; Nilles, J. M.; Radisic, D.; Bowen, K. H. Photoelectron spectroscopy of chromium-doped silicon cluster anions. *J. Chem. Phys.* **2005**, *122*, 071101.

(17) Koyasu, K.; Akutsu, M.; Mitsui, M.; Nakajima, A. Selective formation of MSi_{16} (M = Sc, Ti, and V). *J. Am. Chem. Soc.* **2005**, *127*, 4998−4999.

(18) Koukaras, E. N.; Garoufalis, C. S.; Zdetsis, A. D. Structure and properties of the $Ni@Si_{12}$ cluster from all-electron ab initio calculations. *Phys. Rev. B: Condens. Matter Mater. Phys.* **2006**, *73*, 235417.

(19) Jaeger, J. B.; Jaeger, T. D.; Duncan, M. A. Photodissociation of metal-silicon clusters: encapsulated versus surface-bound metal. *J. Phys. Chem. A* **2006**, *110*, 9310−9314.

(20) Neukermans, S.; Wang, X.; Veldeman, N.; Janssens, E.; Silverans, R. E.; Lievens, P. Mass spectrometric stability study of binary MS_n clusters (S = Si, Ge, Sn, Pb, and M = Cr, Mn, Cu, Zn). *Int. J. Mass Spectrom.* **2006**, *252*, 145−150.

(21) Janssens, E.; Gruene, P.; Meijer, G.; Wöste, L.; Lievens, P.; Fielicke, A. Argon physisorption as structural probe for endohedrally doped silicon clusters. *Phys. Rev. Lett.* **2007**, *99*, 063401.

(22) Grubisic, A.; Wang, H. P.; Ko, Y. J.; Bowen, K. H. Photoelectron spectroscopy of europium-silicon cluster anions, $EuSi_n^-$. *J. Chem. Phys.* **2008**, *129*, 054302.

(23) Koyasu, K.; Atobe, J.; Furuse, S.; Nakajima, A. Anion photoelectron spectroscopy of transition metal- and lanthanide metal-silicon clusters: MSi_n^- (n = 6−20). *J. Chem. Phys.* **2008**, *129*, 214301.

(24) Grubisic, A.; Ko, Y. J.; Wang, H. P.; Bowen, K. H. Photoelectron spectroscopy of lanthanide−silicon cluster anions $LnSi_n^-$ ($3 \le n \le 13$; Ln = Ho, Gd, Pr, Sm, Eu, Yb). *J. Am. Chem. Soc.* **2009**, *131*, 10783−10790.

(25) Lan, Y. Z.; Feng, Y. L. Comparative study on the geometric and energetic properties, absorption spectra, and polarizabilities of charged and neutral $Cu@Si_n$ clusters (n = 9−14). *Phys. Rev. A: At., Mol., Opt. Phys.* **2009**, *79*, 033201.

(26) Lau, J. T.; Hirsch, K.; Klar, P.; Langenberg, A.; Lofink, F.; Richter, R.; Rittmann, J.; Vogel, M.; Zamudio-Bayer, V.; Möller, T.; et al. X-ray spectroscopy reveals high symmetry and electronic shell structure of transition-metal-doped silicon clusters. *Phys. Rev. A: At., Mol., Opt. Phys.* **2009**, *79*, 053201.

(27) Xu, H. G.; Zhang, Z. G.; Feng, Y.; Zheng, W. J. Photoelectron spectroscopy and density-functional study of $Sc_2Si_n^-$ (n = 2−6) clusters. *Chem. Phys. Lett.* **2010**, *498*, 22−26.

(28) Zhao, R. N.; Han, J. G.; Bai, J. T.; Sheng, L. S. The medium-sized charged YSi_n^- (n = 7−13) clusters: a relativistic computational investigation. *Chem. Phys.* **2010**, *378*, 82−87.

(29) Xu, H. G.; Wu, M. M.; Zhang, Z. G.; Sun, Q.; Zheng, W. J. Structural and bonding properties of $ScSi_n^-$ (n= 2−6) clusters: photoelectron spectroscopy and density functional calculations. *Chin. Phys. B* **2011**, *20*, 043102.

DOI: 10.1021/acs.jpcc.6b08598
J. Phys. Chem. C 2016, 120, 25628−25637

(30) Xu, H. G.; Wu, M. M.; Zhang, Z. G.; Yuan, J. Y.; Sun, Q.; Zheng, W. J. Photoelectron spectroscopy and density functional calculations of $CuSi_n^-$ (n = 4−18) clusters. *J. Chem. Phys.* **2012**, *136*, 104308.
(31) Kong, X. Y.; Deng, X. J.; Xu, H. G.; Yang, Z.; Xu, X. L.; Zheng, W. J. Photoelectron spectroscopy and density functional calculations of $AgSi_n^-$ (n = 3−12) clusters. *J. Chem. Phys.* **2013**, *138*, 244312.
(32) Xu, H. G.; Kong, X. Y.; Deng, X. J.; Zhang, Z. G.; Zheng, W. J. Smallest fullerene-like silicon cage stabilized by a V_2 unit. *J. Chem. Phys.* **2014**, *140*, 024308.
(33) Liu, Y.; Li, G. L.; Gao, A. M.; Chen, H. Y.; Finlow, D.; Li, Q. S. The structures and properties of $FeSi_n$ (n = 1−8) clusters. *Eur. Phys. J. D* **2011**, *64*, 27−35.
(34) Holliday, R.; Goodman, P. Going for gold. *IEE. Review* **2002**, *48*, 15−19.
(35) Ishida, T.; Haruta, M. Gold catalysts: towards sustainable chemistry. *Angew. Chem., Int. Ed.* **2007**, *46*, 7154−7156.
(36) Au, V. K. M.; Wong, K. M. C.; Zhu, N. Y.; Yam, V. W. W. Luminescent cyclometalated n-heterocyclic carbene-containing organogold(III) complexes: synthesis, characterization, electrochemistry, and photophysical studies. *J. Am. Chem. Soc.* **2009**, *131*, 9076−9085.
(37) Aragoni, M. C.; Arca, M.; Devillanova, F. A.; Isaia, F.; Lippolis, V.; Pintus, A. Gold(III) complexes of asymmetrically aryl-substituted 1,2-dithiolene ligands featuring potential-controlled spectroscopic properties: an insight into the electronic properties of bis(pyren-1-yl-ethylene-1,2-dithiolato)gold(III). *Chem. - Asian J.* **2011**, *6*, 198−208.
(38) Guenther, J.; Mallet-Ladeira, S.; Estevez, L.; Miqueu, K.; Amgoune, A.; Bourissou, D. Activation of aryl halides at gold(I): practical synthesis of (p, c) cyclometalated gold(III) complexes. *J. Am. Chem. Soc.* **2014**, *136*, 1778−1781.
(39) Kodiyath, R.; Manikandan, M.; Liu, L.; Ramesh, G. V.; Koyasu, S.; Miyauchi, M.; Sakuma, Y.; Tanabe, T.; Gunji, T.; Duy Dao, T.; et al. Visible-light photodecomposition of acetaldehyde by TiO_2-coated gold nanocages: plasmon-mediated hot electron transport via defect states. *Chem. Commun.* **2014**, *50*, 15553−15556.
(40) Johnson, B. T.; Low, R. E.; MacDonald, H. V. Panning for the gold in health research: incorporating studies' methodological quality in meta-analysis. *Psychol. Health.* **2015**, *30*, 135−152.
(41) Pyykkö, P. Relativistic effects in structural chemistry. *Chem. Rev.* **1988**, *88*, 563−594.
(42) Pyykkö, P. Theoretical chemistry of gold. *Angew. Chem., Int. Ed.* **2004**, *43*, 4412−4456.
(43) Zavodinsky, V. G.; Kuyanov, I. A. Schottky barrier formation in a Au/Si nanoscale system: a local density approximation study. *J. Appl. Phys.* **1997**, *81*, 2715−2719.
(44) Madras, P.; Dailey, E.; Drucker, J. Spreading of liquid AuSi on vapor-liquid-solid-grown Si nanowires. *Nano Lett.* **2010**, *10*, 1759−1763.
(45) Dailey, E.; Madras, P.; Drucker, J. Au on vapor-liquid-solid grown Si nanowires: spreading of liquid AuSi from the catalytic seed. *J. Appl. Phys.* **2010**, *108*, 064320.
(46) Matthews, T. S.; Sawyer, C.; Ogletree, D. F.; Liliental-Weber, Z.; Chrzan, D. C.; Wu, J. Q. Large reaction rate enhancement in formation of ultrathin AuSi eutectic layers. *Phys. Rev. Lett.* **2012**, *108*, 096102.
(47) Abe, M.; Nakajima, T.; Hirao, K. A theoretical study of the low-lying states of the AuSi molecule: an assignment of the excited a and d states. *J. Chem. Phys.* **2002**, *117*, 7960−7967.
(48) Sen, P.; Mitas, L. Electronic structure and ground states of transition metals encapsulated in a Si_{12} hexagonal prism cage. *Phys. Rev. B: Condens. Matter Mater. Phys.* **2003**, *68*, 155404.
(49) Chuang, F. C.; Hsu, C. C.; Hsieh, Y. Y.; Albao, M. A. Atomic and electronic structures of $AuSi_n$ (n = 1−16) clusters: A first-principles study. *Chin. J. Phys.* **2010**, *48*, 82−102.
(50) Wang, J.; Liu, Y.; Li, Y. C. Au@Sin: growth behavior, stability and electronic structure. *Phys. Lett. A* **2010**, *374*, 2736−2742.
(51) Li, Y. J.; Lyon, J. T.; Woodham, A. P.; Lievens, P.; Fielicke, A.; Janssens, E. Structural identification of gold-doped silicon clusters via far-infrared spectroscopy. *J. Phys. Chem. C* **2015**, *119*, 10896−10903.
(52) Kiran, B.; Li, X.; Zhai, H. J.; Cui, L. F.; Wang, L. S. $[SiAu_4]$: aurosilane. *Angew. Chem., Int. Ed.* **2004**, *43*, 2125−2129.
(53) Li, X.; Kiran, B.; Wang, L.-S. Gold as hydrogen. An experimental and theoretical study of the structures and bonding in disilicon gold clusters $Si_2Au_n^-$ and Si_2Au_n (n = 2 and 4) and comparisons to Si_2H_2 and Si_2H_4. *J. Phys. Chem. A* **2005**, *109*, 4366−4374.
(54) Kiran, B.; Li, X.; Zhai, H. J.; Wang, L. S. Gold as hydrogen: structural and electronic properties and chemical bonding in $Si_3Au_3^{+/0/-}$ and comparisons to $Si_3H_3^{+/0/-}$. *J. Chem. Phys.* **2006**, *125*, 133204.
(55) Xu, H. G.; Zhang, Z. G.; Feng, Y.; Yuan, J. Y.; Zhao, Y. C.; Zheng, W. J. Vanadium-doped small silicon clusters: photoelectron spectroscopy and density-functional calculations. *Chem. Phys. Lett.* **2010**, *487*, 204−208.
(56) Lee, C.; Yang, W.; Parr, R. G. Development of the colic-salvetti correlation-energy formular into a functional of the electron density. *Phys. Rev. B: Condens. Matter Mater. Phys.* **1988**, *37*, 785−789.
(57) Becke, A. D. Density functional thermochemistry. III. The role of exact exchange. *J. Chem. Phys.* **1993**, *98*, 5648−5652.
(58) Frisch, M. J.; Trucks, G. W.; Schlegel, H. B.; Scuseria, G. E.; Robb, M. A.; Cheeseman, J. R.; Scalmani, G.; Barone, V.; Mennucci, B.; Peterson, K. A.; et al. *Gaussian 09, Revision A.02*; Gaussian, Inc.: Wallingford, CT, 2009.
(59) Dolg, M.; Wedig, U.; Stoll, H.; Preuss, H. Energy adjusted ab initio pseudopotentials for the first row transition elements. *J. Chem. Phys.* **1987**, *86*, 866−872.
(60) Xiao, C. Y.; Hagelberg, F.; Lester, W. A., Jr. Geometric, energetic, and bonding properties of neutral and charged copper-doped silicon clusters. *Phys. Rev. B: Condens. Matter Mater. Phys.* **2002**, *66*, 075425.
(61) Chuang, F. C.; Hsieh, Y. Y.; Hsu, C. C.; Albao, M. A. Geometries and stabilities of Ag-doped Si_n^- (n = 1−13) clusters: a first-principles study. *J. Chem. Phys.* **2007**, *127*, 144313.
(62) Ziella, D. H.; Caputo, M. C.; Provasi, P. F. Study of geometries and electronic properties of $AgSi_n$ clusters using density functional tight binding methods. *Int. J. Quantum Chem.* **2011**, *111*, 1680−1693.
(63) Lv, J.; Wang, Y. C.; Zhu, L.; Ma, Y. M. Particle-swarm structure prediction on clusters. *J. Chem. Phys.* **2012**, *137*, 084104.
(64) Perdew, J. P.; Burke, K.; Ernzerhof, M. Generalized gradient approximation made simple. *Phys. Rev. Lett.* **1996**, *77*, 3865−3868.
(65) Purvis, G. D.; Bartlett, R. J. A full coupled-cluster singles and doubles model: the inclusion of disconnected triples. *J. Chem. Phys.* **1982**, *76*, 1910−1918.
(66) Peterson, K. A.; Figgen, D.; Dolg, M.; Stoll, H. Energy-consistent relativistic pseudopotentials and correlation consistent basis sets for the 4d elements Y-Pd. *J. Chem. Phys.* **2007**, *126*, 124101.
(67) Woon, D. E.; Dunning, T. H. Gaussian basis sets for use in correlated molecular calculations. III. The atoms aluminum through argon. *J. Chem. Phys.* **1993**, *98*, 1358−1371.
(68) Reed, A. E.; Weinhold, F. Natural bond orbital analysis of near-hartree-fock water dimer. *J. Chem. Phys.* **1983**, *78*, 4066−4703.
(69) Reed, A. E.; Weinstock, R. B.; Weinhold, F. Natural population analysis. *J. Chem. Phys.* **1985**, *83*, 735−746.
(70) Reed, A. E.; Weinhold, F. Natural localized molecular orbitals. *J. Chem. Phys.* **1985**, *83*, 1736−1740.
(71) Carpenter, J. E. Extension of Lewis structure concepts to open-shell and excited-state molecular species. PhD. Thesis, University of Wisconsin, Madison, WI, 1987.
(72) Naaman, R.; Vager, Z. *In the Structure of Small Molecules and Ions*; Plenum Press: New York, 1988; pp 1115−1118.
(73) Reed, A. E.; Curtiss, L. A.; Weinhold, F. Intermolecular interactions from a natural bond orbital, donor-acceptor viewpoint. *Chem. Rev.* **1988**, *88*, 899−926.
(74) Carpenter, J. E.; Weinhold, F. Analysis of the geometry of the hydroxymethyl radical by the "different hybrids for different spins" natural bond orbital procedure. *J. Mol. Struct.: THEOCHEM* **1988**, *169*, 41−62.

DOI: 10.1021/acs.jpcc.6b08598
J. Phys. Chem. C 2016, 120, 25628−25637

(75) Cui, L. F. Photoelectron spectroscopy studies on group IV semiconductor clusters and novel binary clusters. PhD. Thesis, Washington State University, 2007.
(76) Tozer, D. J.; Handy, N. C. Improving virtual kohn−sham orbitals and eigenvalues: application to excitation energies and static polarizabilities. *J. Chem. Phys.* **1998**, *109*, 10180−10189.
(77) Akola, J.; Manninen, M.; Hakkinen, H.; Landman, U.; Li, X.; Wang, L. S. Photoelectron spectra of aluminum cluster anions: Temperature effects and ab initio simulations. *Phys. Rev. B: Condens. Matter Mater. Phys.* **1999**, *60*, R11297.
(78) Kong, X. Y.; Xu, H. G.; Zheng, W. J. Structures and magnetic properties of $CrSi_n^-$ (n = 3−12) clusters: photoelectron spectroscopy and density functional calculations. *J. Chem. Phys.* **2012**, *137*, 064307.
(79) Ho, K.-M.; Shvartsburg, A. A.; Pan, B. C.; Lu, Z. Y.; Wang, C. Z.; Wacker, J. G.; Fye, J. L.; Jarrold, M. F. Structures of medium-sized silicon clusters. *Nature* **1998**, *392*, 582−585.
(80) Lu, S. J.; Hu, L. R.; Xu, X. L.; Xu, H. G.; Chen, H.; Zheng, W. J. Transition from exohedral to endohedral structures of $AuGe_n^-$ (n = 2−12) clusters: photoelectron spectroscopy and ab initio calculations. *Phys. Chem. Chem. Phys.* **2016**, *18*, 20321−20329.
(81) Scherer, J. J.; Paul, J. B.; Collier, C. P.; O'Keefe, A.; Saykally, R. J. Cavity ringdown laser absorption spectroscopy and time-of-flight mass spectroscopy of jet-cooled gold silicides. *J. Chem. Phys.* **1995**, *103*, 9187−9192.
(82) Neckel, A.; Sodeck, G. Bestimmung der dissoziationsenergien der gasfiirmigen molekiile CuGe, AgGe und AuGe. *Monatsh. Chem.* **1972**, *103*, 367−382.
(83) Gingerich, K. A. Gaseous metal silicides. I. Dissociation energy of the molecule AuSi. *J. Chem. Phys.* **1969**, *50*, 5426−5428.
(84) Schmude, R. W., Jr.; Ran, Q.; Gingerich, K. A.; Kingcade, J. E., Jr. Atomization enthalpy and enthalpy of formation of gaseous Si_2 and Si_3 from mass spectrometric equilibrium measurements. *J. Chem. Phys.* **1995**, *102*, 2574−2579.
(85) Willis, M.; Gotz, M.; Kandalam, A. K.; Gantefor, G. F.; Jena, P. Hyperhalogens: discovery of a new class of highly electronegative species. *Angew. Chem., Int. Ed.* **2010**, *49*, 8966−8970.
(86) Feng, Y.; Xu, H. G.; Zheng, W. J.; Zhao, H. M.; Kandalam, A. K.; Jena, P. Structures and photoelectron spectroscopy of $Cu_n(BO_2)_m^-$ (n, m = 1, 2) clusters: observation of hyperhalogen behavior. *J. Chem. Phys.* **2011**, *134*, 094309.
(87) Kong, X. Y.; Xu, H. G.; Koirala, P.; Zheng, W. J.; Kandalam, A. K.; Jena, P. Identification of hyperhalogens in $Ag_n(BO_2)_m$ (n = 1−3, m = 1−2) clusters: anion photoelectron spectroscopy and density functional calculations. *Phys. Chem. Chem. Phys.* **2014**, *16*, 26067−26074.
(88) Chen, H.; Kong, X. Y.; Zheng, W. J.; Yao, J. N.; Kandalam, A. K.; Jena, P. Anomalous property of $Ag(BO_2)_2$ hyperhalogen: does spin-orbit coupling matter? *ChemPhysChem* **2013**, *14*, 3303−3308.
(89) Clementi, E.; Raimondi, D. L.; Reinhardt, W. P. Atomic screening constants from scf functions. II. Atoms with 37 to 86 electrons. *J. Chem. Phys.* **1967**, *47*, 1300−1307.
(90) Scherer, J. J.; Paul, J. B.; Collier, C. P.; Saykally, R. J. Cavity ringdown laser absorption spectroscopy and time-of-flight mass spectroscopy of jet-cooled silver silicides. *J. Chem. Phys.* **1995**, *103*, 113−120.
(91) Pauling, L. *The Nature of the Chemical Bond*; Cornell University Press: Ithica, NY, 1960; pp 88−107.

DOI: 10.1021/acs.jpcc.6b08598
J. Phys. Chem. C 2016, 120, 25628−25637